INDERSCIENCE PUBLISHERS
Linking academia, business and industry through research

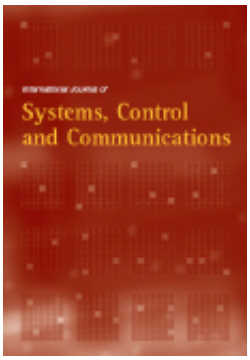

International Journal of Systems, Control and Communications

ISSN online: 1755-9359 - ISSN print: 1755-9340
https://www.inderscience.com/ijscc

Decentralised adaptive fuzzy sliding mode control for robotic arms using a voltage control approach in workspace

Li Wang

DOI: 10.1504/IJSCC.2025.10072074

Article History:

Received:	26 April 2025
Last revised:	15 May 2025
Accepted:	28 May 2025
Published online:	30 October 2025

Decentralised adaptive fuzzy sliding mode control for robotic arms using a voltage control approach in workspace

Li Wang

School of Mechanical Engineering,
Chongqing Industry Polytechnic University,
Chongqing, 400020, China
Email: cqipcwangly@163.com

Abstract: The paper presents a novel decentralised adaptive fuzzy sliding mode control (AFSMC) strategy with voltage-based control for robotic arms operating in the workspace. Traditional torque-based methods require precise dynamic modelling and are often too computationally intensive for real-time or embedded applications. The proposed approach directly manipulates motor voltage inputs, simplifying control law derivation while ensuring robustness against uncertainties, unknown dynamics, and external disturbances. By integrating fuzzy logic approximators within the sliding mode framework, the method effectively compensates for structural and non-structural uncertainties, eliminating the need for accurate dynamic models. A hyperbolic tangent function is employed to reduce chattering and achieve smoother control signals. Furthermore, the workspace-based design addresses end-effector trajectory limitations inherent in joint-space controllers. Simulation results for a three-degree-of-freedom manipulator demonstrate high tracking precision, excellent disturbance rejection, and lower computational demand, making the proposed voltage-based AFSMC highly suitable for real-time industrial and collaborative robotic applications.

Keywords: robotic arm control; voltage control tactic; adaptive fuzzy sliding mode control; AFSMC.

Reference to this paper should be made as follows: Wang, L. (2025) 'Decentralised adaptive fuzzy sliding mode control for robotic arms using a voltage control approach in workspace', *Int. J. Systems, Control and Communications*, Vol. 16, No. 6, pp.1–20.

Biographical notes: Li Wang received her Master's in Pattern Recognition and Intelligent System major from Chongqing University in 2007. Currently, she works in Chongqing Industry Polytechnic University as an Associate Professor. Her research interests include industrial management system and remote sensing data processing.

1 Introduction

Robotic arms are vital in industry and perform some industrial tasks quickly and accurately. One of the essential reasons for using robotic arms is to reduce the cost of production, improve quality accuracy, and increase production, which has more flexibility in performing various tasks compared to other specialised machines Jin et al.

(2024). Electric motors power most robots. On the other hand, robot joints require high torque and move at a low speed. As a result, motors are equipped with a power transmission system to move the robot (Behnamfar et al., 2024; Ur Rahman Efti et al. 2023). To do anything, the robot must be controlled. The proportional-integral-derivative control is one of the most often utilised classical controllers in the robot's joint space. By expanding research in this field, researchers have proven that proportional integral derivative (PID) controllers are simple and implementable Ariyansyah and Ma'arif (2023). Also, they are stable and resistant to the uncertainties of the robotic arm in point-setting mode. Subsequently, separate joint control strategies were employed, including this method and the proportional-derivative control method with gravitational moment compensation. These conventional methods were utilised for controlling the position of the robotic arm. Multi-input, multi-output is how the robotic system operates. The controller design is complicated by nonlinear disturbances from outside the system, coupling in the dynamics of the robotic arm, and uncertainty in the robot model, all of which make control goals more difficult to achieve Yang et al. (2023)

1.1 Related work

The new composite nonlinear feedback (U-CNF) method based on U-control was presented by Zhu et al. (2023) and has been designed around the double feedback loop setup. An inner loop keeps the system stabilised and cancels out nonlinearities utilising dynamic inversion, while an outer loop improves a monotonic nonlinear function for the transient response. This model-independent control strategy is robust to uncertainty as well as external disturbances, and applies to general nonaffine nonlinear systems. Simulations validate its efficacy and offer a clear framework for practical applications. Ruderman (2023) studied several aspects of kinetic friction in the field of robotics and control systems, providing an exhaustive coverage ranging from characteristics, effects on motion dynamics, and approaches for compensation. Theoretical concepts, modelling energy dissipation, and practical control techniques, including observers, are discussed, and the book should serve as a source of guidance for students and professionals in robotics and mechatronics. Mohammadi et al. (2021) reviewed control strategies for robust AC, DC, and hybrid microgrids integrated with PV and wind power. The paper discussed some of the key control objectives: voltage and frequency support and power sharing, and it compares the methods under consideration having different microgrid topologies. The paper describes the research gaps found in characterisation, robustness evaluation, and assessment techniques and proposes some solutions as support for future developments in microgrid control.

Liu et al. (2021) proposed an adaptive motion control method for robotic manipulators, uses an RBF neural network. The model approximates the unknown nonlinear function while ensuring stability for the motion of the system, as proved by the Lyapunov function. An RBF-based terminal sliding mode controller with a backstepping approach is incorporated within the neurosystem to gain improvement in adaptivity. The proposed control method realises fine and stable manipulator operations in logistics and agricultural applications, displaying a high degree of flexibility and robustness in complex motion tasks. Odry et al. (2020) have carried this out via the implementation of a low-cost self-balancing robot (SBR) to afford students hands-on training in the whole process of control system design, starting from modelling and simulation in MATLAB/Simulink to real-time implementation. Fuzzy logic (FLC) control is thereby

used alongside a more conventional approach of coding-control by means of a lookup table. Such a control strategy is expected to promote a deeper understanding of the topic of feedback control, owing to the interaction and development in good practical work of students. Kumar and Kumar (2021) provided a review of controller strategies for two-link robotic manipulators, contrasting conventional PID controllers with intelligent methods such as FLC and artificial neural networks (ANN), thereby optimising using genetic algorithms (GA). While PID is simple and inexpensive, it becomes ineffective when the system is subjected to nonlinearities and uncertainties.

The review highlights the trend towards employing soft-computing techniques for greater robustness and better control accuracy in today's robotics. Moudoud et al. have proposed a fuzzy adaptive sliding mode controller (FASMC) for trajectory tracking in wheeled mobile robots that operate under uncertainties and disturbances. This method comprises a finite-time kinematic controller executed in conjunction with dynamic FASMC to achieve closed-loop stability, robust tracking, and diminished chattering. FLC makes the system adaptable, while Lyapunov analysis holds that the system is stable. The controller's effectiveness has been validated by simulation results in MATLAB/Simulink. Nekoukar and Dehkordi (2021) develop a resilient quadrotor flight control system utilising an adaptive fuzzy terminal sliding-mode controller in combination with PD controllers. The system stabilises the quadrotor and tracks predefined paths even under the effects of disturbance and uncertainty. Adaptive Mamdani fuzzy systems recognise the system dynamics in real-time discrimination, while a continuous sliding mode permits reduced chattering. Kalman filters will optimise both attitude and position estimation. Simulations and real-time tests prove the effectiveness of such controllers. Yin et al. (2021) studied forth a robust AFSMC strategy, effectively designed for trajectory tracking of uncertain serial robotic manipulators.

The method does sliding mode control with FLC approximation and thus compensates for high-frequency uncertainties and makes real-time adaptation for low-frequency variations. The comparison tests conducted show improved tracking accuracy and robustness to disturbances compared to those of standard controllers. Abdel-Sattar et al. (2025) conducted a comparative analysis of the control of single-joint robotic arms using an optimal sliding surface PID (SSPID) controller optimised by particle swarm optimisation. The SSPID controller combines sliding mode control and PID control for better disturbance-rejection; the authors found that the SSPID controller has superior tracking accuracy, rise time, and stability than PID and FOPID under different parameter variations. According to Fazilat et al. (2025) a sliding-mode control based on quantum mechanisms will enhance the robustness, accuracy, and efficiency of systems in robotics. Q-SMC, which is applied to a six-joint articulated robotic manipulator, solves the classical problems encountered in sliding-mode control, namely, chattering and high computational load. The simulation results show that the Q-SMC achieves improved tracking accuracy compared to the conventional method, saving energy consumption by ~3.79%. This necessitates further investigation into the application of Q-SMC for high-precision robotic control.

1.2 Research gap

Although there have been advancements in adaptive and intelligent control, the majority of the existing frameworks around AFSMC rely on torque-level control that assumes knowledge of the exact robot dynamics and therefore requires mapping torque to voltage.

This dependency on exact models adds to the computational complexity of such controllers and, more to the point, limits their applicability in real-time situations, particularly in embedded systems or resource-constrained environments. Last but not least, workspace-level control, a requirement for end-effector accuracy, had so far been hampered by some Jacobian matrices, which, in turn, can seldom give reasonable results in the face of joint velocity discrepancies or mechanical inconsistencies. Then there are more uncertainties like parametric uncertainties, dry friction, and unmodelled dynamics that further damage control performance in any torque-based control.

1.3 Novelty

For the first time, this study intends to fill the above gaps by proposing a decentralised AFSMC associated with a voltage control strategy for robotic arms in their workspace. The proposed method directly controls motor voltages and therefore significantly simplifies the control structure, eliminating model-based torque computation requirements and also reducing computational demands.

Key contributions of this study include:

- The development of a voltage-AFSMC scheme that does not require complete dynamic modelling or torque estimation.
- Integrating FLC approximators into sliding mode control to cope with structural and non-structural uncertainties, while reducing overall chattering of control signals through a hyperbolic tangent smoothing approach.
- A complete workspace-level control formulation with Jacobian-based feedback, compensating for kinematic transformation inaccuracies.
- Simulation results of the proposed approach on a 3-DOF robotic arm show that this method offers better tracking accuracy and disturbance rejection, as compared to conventional torque-based controllers.

The rest of the paper is organised as follows: Section 2 describes robot modelling, while Section 3 discusses workspace control, and Section 4 presents the proposed control law. Section 5 presents a simulation result analysis, while Section 6 presents the discussion, and Section 7 gives the conclusions.

2 Modelling

An important step in building an effective controller for a robotic arm is to obtain a dynamic model describing accurately describes the physical behaviour of the mechanical structure and its actuators. In this study, the articulation and control development are based on the Lagrangian formulation, considering the robotic arm as a multi-degree-of-freedom system using permanent magnet DC motors in the driving system. The dynamics are characterised as severely nonlinear and coupled due to inertial effects, Coriolis and centrifugal forces, gravitational torques, dry friction, and external disturbances. The robot's dynamic equations can be explained as Fateh et al. (2009):

$$D(\theta)\ddot{\theta} + C(\theta, \dot{\theta})\dot{\theta} + G(\theta) + F_s(\dot{\theta}) = \tau \tag{1}$$

where the robotic arm's inertia matrix is denoted by D, the gravitational force vector is represented by G, the input torque vector is represented by τ, the joint variables are represented by θ, the joint velocities and accelerations are represented by $\dot{\theta}$ and $\ddot{\theta}$, respectively. The dry friction terms are represented by F_s, and C is the vector of Coriolis moments and the centre side. The torques produced by electric motors follow equation (2):

$$J\ddot{\theta}_m + B\dot{\theta}_m + r\tau = \tau_m \tag{2}$$

τ_m displays the torque vector of the motors, θ_m displays the position vector of the motors, r is the gear reduction factor, and J and B are the motor parameters. According to equation (3), the motors' speed vector and the robot's Jacobian matrix vector are used. In the absence of speed, the joints are related to each other:

$$r\dot{\theta}_m = \dot{\theta} \tag{3}$$

Equations (1) and (2) are strongly nonlinear and coupled. The use of permanent magnet DC motors is common in robotic applications. Since the pole flux is constant in this motor, the behaviour analysis and motor equations are simplified. The armature coil is located on the rotor (moving part), and constant flux is created by permanent magnets installed in the stator (fixed part). By applying voltage to the motor, the armature coil carries current. Due to the force applied to the current-carrying wire in the magnetic field, the torque resulting from applying force to the armature coil rotates the rotor. This torque is a function of pole flux and armature current. Since the pole flux is constant, the created torque is proportional to the armature current. The torque vector of motors τ_m is expressed as follows:

$$K_m I_\alpha = \tau_m \tag{4}$$

where the constant diagonal matrix, K_m, and the motor current, $I_\alpha \in R^n$, are given. As a result of the rotation of the armature in the magnetic field, a voltage that opposes the current is induced in the armature. This voltage is a function of pole flux and rotation speed. Since the pole flux in this motor is constant, this voltage is proportional to the velocity of the motor, so the matrix equation of the motor armature coil voltage is as follows:

$$RI_\alpha + LI_{\dot{\alpha}} + K_b\dot{\theta}_m = u \tag{5}$$

R displays the ohmic resistance matrix of the armature coil, L displays the inductance matrix of the armature coil, and K_b displays the constant matrix of the inductive anti-excitation and the input voltage vector of the motors. Equations (1) to (5) are written in the state space form:

$$\dot{z} = f(z) + bu \tag{6}$$

u is the input voltage vector of the motors, $f(z)$, b, and z are obtained as follows:

$$\begin{aligned} f(z) = \Big[\left(Jr^{-1} + rD(z_1)\right)^{-1} \left(Br^{-1} + rC(z_1, z_2)\right) z_2 - rG(z_1) \\ -rF(z_2) + K_m z3 \Big] - L^{-1}\left(K_b r^{-1} z_2 + Rz3\right) \end{aligned} \tag{7a}$$

$$b = \begin{bmatrix} 0 \\ 0 \\ L^{-1} \end{bmatrix} \tag{7b}$$

$$z = \begin{bmatrix} \theta \\ \dot{\theta} \\ I_\alpha \end{bmatrix} \tag{7c}$$

3 Work space control

Given the external disturbance of $\varphi(t)$, equation (5) is modified by inserting equation (3) in equation (5) as follows:

$$RI_\alpha + LI_{\dot{\alpha}} + K_b\dot{\theta}_m + \varphi(t) = u \tag{8}$$

The direct kinematics of the robot is defined as equation (8):

$$X = F(\theta) \tag{9}$$

X displays the coordinates of the final robot executive, and F is the mapping between the workspace X and the joint space θ. The coordinate system with the robot's joint positions as its axes is called the joint space θ, and the coordinate system with the robot's ultimate executive position as its axes is called the workspace X. By deriving equation (9) concerning time, the equation below is obtained:

$$\dot{X} = J(q)\dot{q} \tag{10}$$

$J(q)$ is called the Jacobian matrix. By inserting equation (10) in equation (7) and simplifying, the equation below is obtained:

$$X = -J(\theta)rK_b^{-1} + RI_\alpha + J(\theta)rK_b^{-1}u + M \tag{11}$$

$$M = J(\theta)rK_b^{-1}\left(LI_{\dot{\alpha}} + \varphi(t)\right) \tag{12}$$

In this case, $LI_{\dot{\alpha}}$ is considered to be an unmodelled dynamic. To simplify, equation (10) is formulated as:

$$\dot{X} = F + Gu + M \tag{13}$$

$$F = J(\theta)rK_b^{-1}RI_\alpha,\ G = J(\theta)rK_b^{-1} \tag{14}$$

4 Recommended control law

Although the robot's dynamic equations are intricate and include numerous inputs and multiple outputs, the electric motor may be represented as a single-input, single-output system. Because of this, the voltage control technique serves as the foundation for the

suggested control method. To suggest the control law, the following nominal model based on equation (11) is suggested:

$$X = -\hat{J}(\theta)\hat{r}\hat{K}_b^{-1}\hat{R}I_\alpha, \hat{J}(\theta)\hat{r}\hat{K}_b^{-1}u \tag{15}$$

The system's nominal model is well-established and founded on a thorough understanding of its dynamics. The development and use of control techniques are based on this concept. $J(\theta)$, r, $\boldsymbol{K}_b$, and $\boldsymbol{R}$ are the corresponding values in order of estimation. Equation (11) is rewritten as equation (16) by considering the nominal values:

$$X = -\hat{J}(\theta)\hat{r}\hat{K}_b^{-1}\hat{R}I_\alpha + \hat{J}(\theta)\hat{r}\hat{K}_b^{-1}u + d \tag{16}$$

where d is the integrated uncertainty. Equation (16) is simply formed:

$$\dot{X} + F_1 + G_1 u + d \tag{17}$$

$$F_1 = \hat{J}(\theta)\hat{r}\hat{K}_b^{-1}\hat{R}I_\alpha, G_1 = \hat{J}(\theta)\hat{r}\hat{K}_b^{-1}u \tag{18}$$

Using the feedback linearisation method and considering $d = 0$, the control law is recommended as the following relationship:

$$u = G_1^{-1}\left(-F_1 + \dot{X}_d - \alpha\left(X - X_d\right)\right) \tag{19}$$

X_d represents the ideal location in the workspace, while α is a positive-definite diagonal constant matrix. Substituting equation (19) in equation (17), performing calculations, and considering $d = 0$, the equation below is obtained:

$$\dot{e} + \alpha e = 0 \tag{20}$$

where e, which may be calculated as $e = X–X_d$, represents the tracking error. Using the control law equation (19), the error tends to be zero. The functions G_1 and F_1 are known. In the absence of uncertainties, the feedback linearisation method will be useful. But in the presence of uncertainties, the system's performance is weakened. The following equation is suggested as a workaround for the sliding mode's fuzzy control law:

$$u = G_1^{-1}\left[u_1 + u_2\right] \tag{21}$$

where u_1 is the sliding mode part, and u_2 is the phase part. In this research, the sliding mode section is suggested:

$$u_1 = \dot{X}_d - \alpha e - sgn(S)(P + \mu) \tag{22}$$

where α is the positive-definite diagonal constant matrix, P is the estimation vector of uncertainty limits, and μ is the vector of positive constant values.

$$S = X - X_d + \alpha\int\left(X - X_d\right)dt \tag{23}$$

Also, the fuzzy part considering the fuzzy making is suggested as follows:

$$u_2 = -\xi_f\theta_f = \begin{bmatrix} \xi_{f1} & \cdots & 0 \\ \vdots & \ddots & \vdots \\ 0 & \cdots & \xi_{f1} \end{bmatrix}\begin{Bmatrix} \theta_{f1} \\ \vdots \\ \theta_{fn} \end{Bmatrix} \tag{24}$$

According to the general approximation theorem Nguyen and Sugeno (2012), there exists a fuzzy system such that:

$$F_1 = \xi_f \theta_f + \varepsilon \tag{25}$$

where the vector ε indicates the bounded approximation error. The estimation of the uncertainty limit vector and the parameters of the fuzzy system are done below: The derivative in equation (23) concerning time becomes:

$$\dot{S} = \dot{X} - \dot{X}_d + \alpha e \tag{26}$$

Changing equations (22) and (24) into equation (21) and then inserting equations (20) and (25) into equation (17), it follows:

$$\dot{X} = \xi_f \left(\theta_f + \hat{\theta}_f \right) + \dot{X}_d - \alpha e - sgn(S)(P + \mu) + d + \varepsilon \tag{27}$$

Inserting equation (27) into equation (26) yields:

$$\dot{S} = \xi_f \hat{\theta}_f + d + \varepsilon - sgn(S)(P + \mu) \tag{28}$$

The Lyapunov function is chosen as equation (29) to prove stability and obtain the parameter update rules.

$$V = 05 S^T S + 1 \frac{\theta_f^T \theta_f}{2\gamma_1} + 1 \frac{P^T P}{2\gamma_1} \tag{29}$$

The coefficients γ_1 and γ_2 are positive and constant. By deriving the above relationship, the equation below is obtained:

$$\dot{V} = S^T \dot{S} + 1 \frac{\dot{\theta}_f^T \theta_f}{\gamma_1} + 1 \frac{\dot{P}^T P}{\gamma_1} \tag{30}$$

By inserting equation (28) into equation (30) and simplifying it, the equation below is obtained:

$$\dot{V} = \left(S^T \xi_f - 1 \frac{\dot{\theta}^T}{\gamma_1 f} \right) \theta_f + \left(S^T sgn(S) \frac{-1}{\gamma_1} \dot{P}^T \right) P + S^T (\varepsilon + d) - S^T sgn(S) \hat{P} - S^T sgn(S) \mu \tag{31}$$

Now, matching rules are defined as the following relations:

$$\dot{\theta}_f^T = \gamma_1 S^T \xi_f \tag{32}$$

$$\dot{P}^T = \gamma_2 S^T sgn(S) \tag{33}$$

Therefore, the parameters are calculated as:

$$\dot{\theta}_f(t) = \dot{\theta}_f(0) + \gamma_1 \int_0^t S^T \xi_f dt \tag{34}$$

$$\dot{P}(t) = \dot{P}(0) + \gamma_2 \int_0^t S^T sgn(S) dt \tag{35}$$

By inserting matching rules, equations (32) and (33) in equation (31), the equation below is obtained:

$$\dot{V} \leq -S^T sgn(S)\mu \tag{36}$$

Therefore, the convergence of S to zero is guaranteed. The diagram of the recommended control system is drawn in Fig. 1.

Figure 1 Flowchart of the recommended control system (see online version for colours)

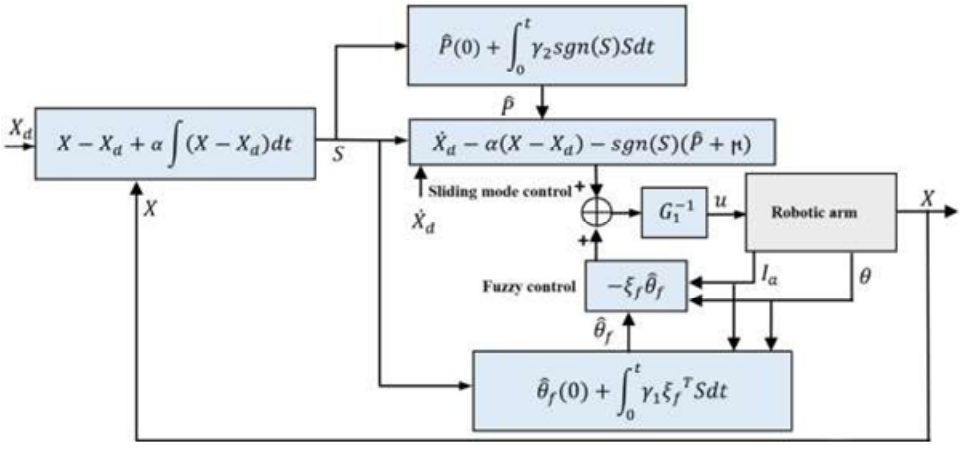

To reduce the vibration of the control signal, instead of the sign function $sgn(S)$, the hyperbolic tangent function $tanh(yS)$ can be used Hu et al. (2008), which has a positive coefficient. In this case, the resulting control law is a continuous approximation of the previous discontinuous control law, which, while reducing the vibration of the control signal, also slightly weakens it. Because the asymptotic convergence of the error to zero is not achieved, the convergence will be final in the form of a uniform boundary. In practice, control rules are programmed and stored as programs in the controller. It is possible to convert mathematical equations into a program, but it is necessary to complete all calculations in a short sampling time. The higher the speed of the processor, the shorter the calculation time. Since the recommended control is independent of the model, it has fewer calculations than the model-based control method. Another practical issue is that the signals needed by the controller are available and measurable. The suggested design takes advantage of the accessible and measurable feedback provided by the motor current I_α, the ultimate actuator position X, and the joint position θ.

5 Simulation

3 hinged joints of the artist robot are used to replicate the suggested control scheme. Reference Fateh et al. (2012) shows an overview of this robot. The parameters of the robot utilising the Denavit-Hartenberg method are listed in

Table 1, where α_1, d_i, θ_i, and α_i express length, deflection, angle, and twist accordingly. The engine metrics are listed in Table 2. The desired routes are displayed in Figures 2 and 3, respectively.

Table 1 Robot parameters with the Denavit-Hartenberg method

Axis	*a*	*d*	*θ*	*α*
1	0	d1	θ1	π/2
2	a2	0	θ2	0
3	a3	0	θ3	0

Table 2 Motor parameters

Motors	*R*	*B*	*J*	*L*	*Kb*	*r*
1, 2, 3	0.05	0.002	0.00006	0.003	0.35	2.03

Figure 2 The desired trajectory for the first and second components of the final executive (see online version for colours)

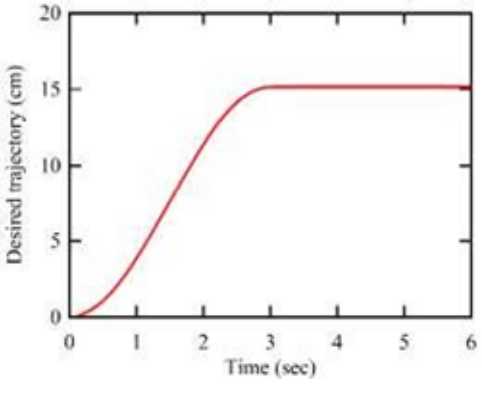

Also, the disturbance considered in this simulation is displayed in Fig. 4. The amount of disturbance is about 25% of the maximum voltage applied to the joints. $F_s(\theta)$ in equation (1) is as follows:

$$F_s(\dot{\theta}) = \begin{Bmatrix} 2\dot{\theta}_1 + 8sgn(\dot{\theta}_1) \\ 4\dot{\theta}_2 + 16sgn(\dot{\theta}_2) \\ 4\dot{\theta}_2 + 8sgn(\dot{\theta}_3) \end{Bmatrix} \tag{37}$$

Figure 3 The desired trajectory for the third component of the final executive (see online version for colours)

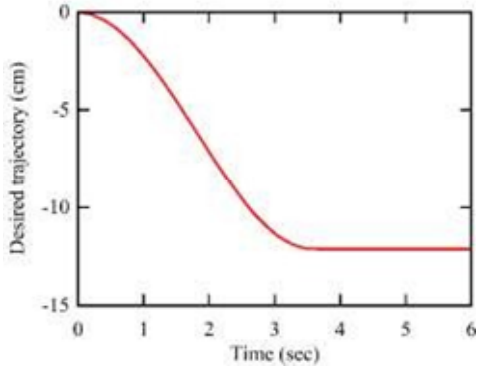

Figure 4 External disturbance to the motor of each joint (see online version for colours)

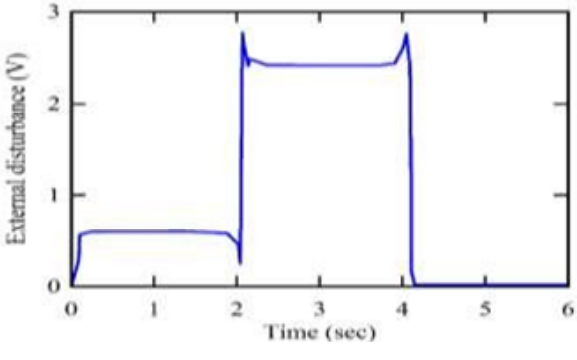

Figure 5 The initial part of the ultimate executive's tracking inaccuracy (see online version for colours)

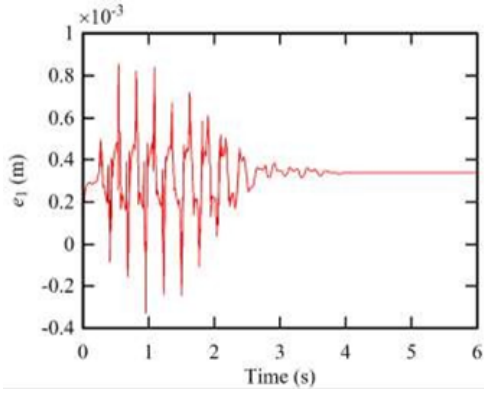

Figure 6 The tracking error of the second component of the final executive (see online version for colours)

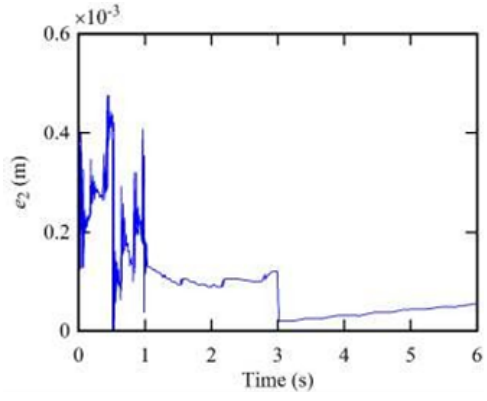

Figure 7 Tracking error of the third component of the final executive (see online version for colours)

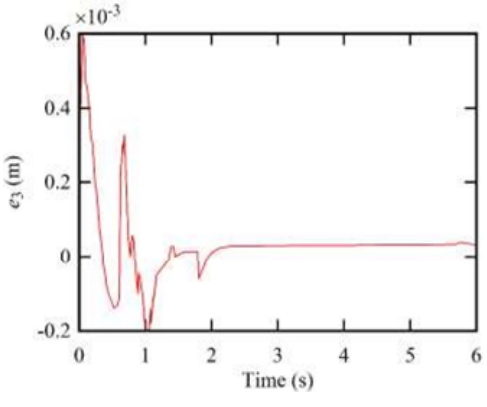

The system's productivity is displayed in Figures 5 to 7. As it is perceivable, the tracking is done well. The tracking error of the first component of the final operator, which is displayed in Figure 5, has reached 0.82×10^{-3} rad, and the percentage of the error ratio to the signal has reached 1.3%. The tracking error of the second component of the final executive in the figure has reached 1.4×10^{-3} rad, and the percentage of the error ratio to the signal has reached 0.54%. The tracking error of the third component, the final operator in Figure 7, has reached 2.1×10^{-3}, and the percentage of the error ratio to the signal has reached 1.2%. Also, the control signals of the 3 joints are displayed in Figure 8, which indicates these signals are within the allowed range. The simulation outcomes show the efficacy of the control tactic in the presence of external disturbance and dry friction.

Figure 8 The control signal of the first, second, and third joints (see online version for colours)

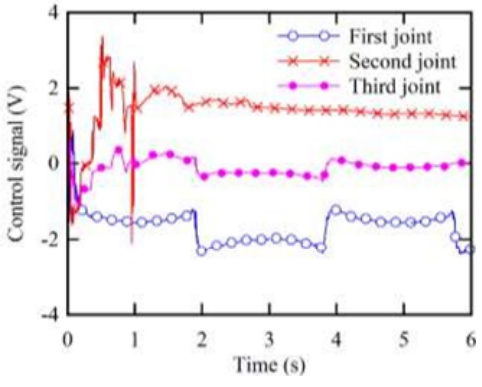

Figure 9 An external disturbance is applied to the system (see online version for colours)

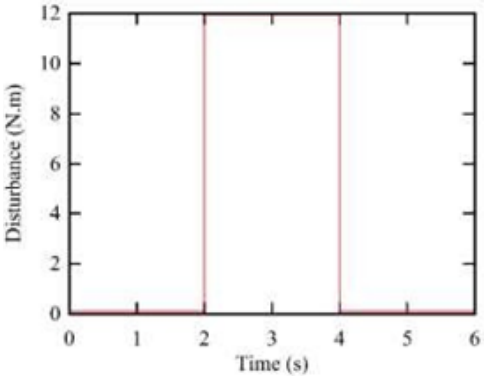

Figure 10 The torque control method's first, second, and third component tracking errors (see online version for colours)

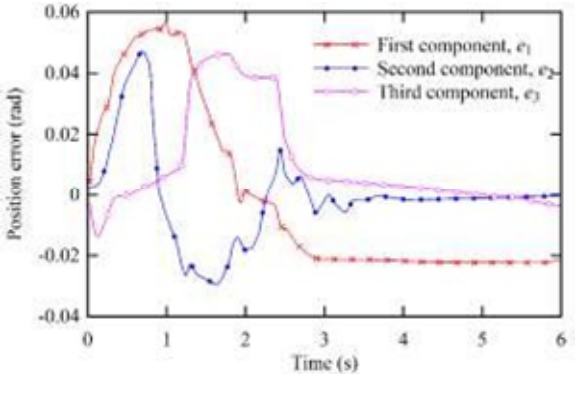

As stated in Section 2, adaptive fuzzy sliding control methods for robotic arms in joint space based on torque are presented in Refs. Sharkawy et al. (2011) and Ho et al. (2007). To compare the recommended tactic with those drawing on the torque control tactic, the simulation of the method described in the reference is Ho et al. (2007) is performed on the artist robot. The friction vector is considered as per equation (35), and the external disturbance, illustrated in Figure 9, is set to 25% of the maximum torque applied to the joints. Figure 10 displays the tracking errors, and Figure 11 displays the joint torque control signals. The tracking error of the first component of the final executive in Figure 10 has reached 0.058 rad, and the percent error to the signal has reached 14%. The tracking error of the second component of the final executive has reached 0.045 rad, and the percentage of the error size to the signal has reached 15%. Also, the tracking error of the third component of the final executive has reached 0.049 rad, and the percentage of the error size to the signal has reached 2%. Examining and comparing the outcomes reveals that the tracking error of the recommended tactic is notably lower than that of the tactic in Ho et al. (2007). Also, the control complications in the voltage control strategy are much less than in the torque control strategy.

Figure 11 (a) control torque of the first joint (b) control torque of the second joint and (c) control torque of the third joint

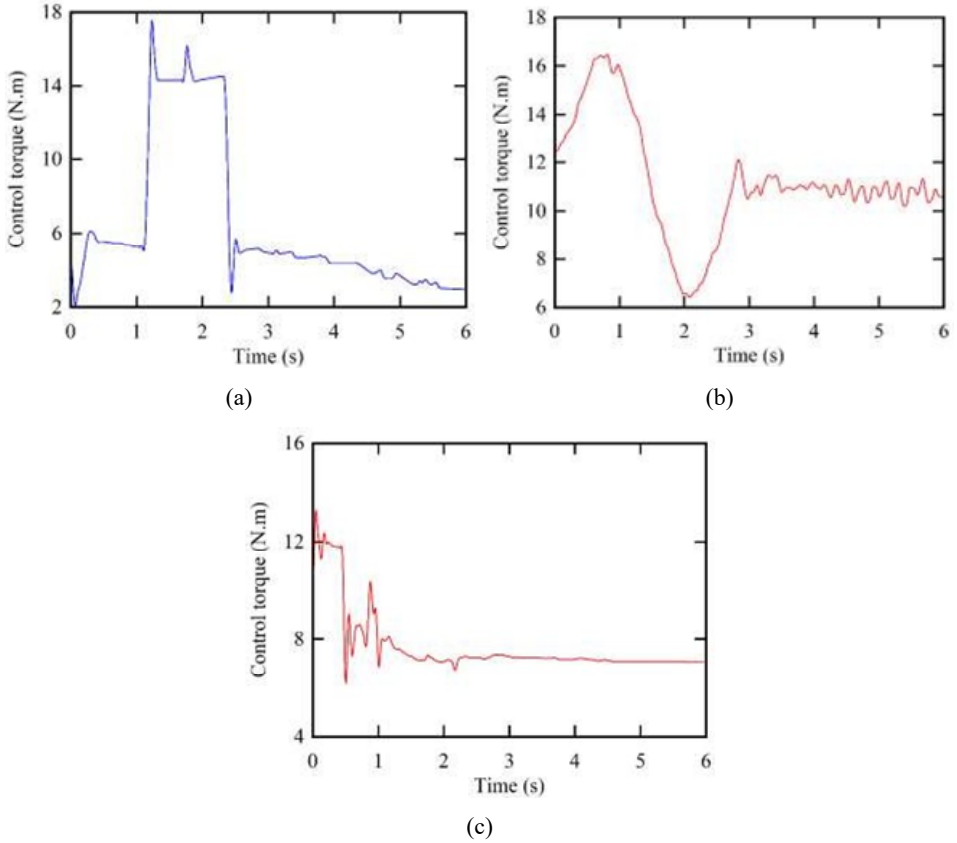

6 Discussion

The simulation results from Section 5 validate the theoretical design and verify the robustness and effectiveness of the proposed AFSMC using a voltage control strategy for robotic arm control in the workspace. This method outperforms common torque-based control schemes in tracking accuracy and disturbance rejection by a wide margin, along with less computation overhead.

6.1 Evaluation of performance and accuracy

The proposed AFSMC is extremely accurate in trajectory tracking. The final actuator components showed maximum steady-state tracking errors of 0.82×10^{-3}, 1.4×10^{-3}, and 2.1×10^{-3} radians with the corresponding signal-related error percentages of 1.3%, 0.54%, and 1.2%. These error values are considerably lower than those of the torque – based controller tracking error measured in Ref. Ho et al. (2007). At maximum, the tracking errors reached up to about 0.058 rad with up to 15% of relative error. However, these results prove that the method is capable of high-precision control in the workspace while being relatively insensitive to parametric and structural variations that tend to impair that precision in model-based techniques.

6.2 Robustness against uncertainties and disturbances

Robustness is a central design objective of the AFSMC. The simulation setup includes external disturbances equivalent to 25% of the maximum control signal, along with dry friction modelled through $F_s(\theta)$. Despite these non-ideal conditions, the proposed controller maintained system stability and acceptable tracking performance without requiring explicit disturbance modelling or additional observers. Lyapunov-based adaptive laws derive mathematically guaranteed robustness in Section 4. The control law approximates uncertainty bounds using fuzzy systems equation (24) and includes various adaptations equations (32)–(35), thus ensuring that uncertainties d and approximation errors $\in$ are bounded and compensated in real-time.

6.3 Model-free advantage and computational simplicity

Additionally, the proposed control strategy is based on the nominal motor voltage equation (16), requiring no precise knowledge of the inertia matrix of the robot, the Coriolis terms, or the gravity vector to develop control strategies. This renders the system as a single-input single-output (SISO) structure for each motor and makes the approach favourable towards embedded control applications that may not have the best processing capabilities.

By directly controlling the workspace. the problem of joint-space-based controllers, which fail to guarantee the proper end-effector due to transformation errors in the Jacobian matrix and unobservable interactions between joints, is eliminated. The proposed method thus provides workspace feedback directly, remedying this inadequacy.

6.4 Sliding mode behaviour and smoothed control signals

SMC was famous for creating chattering because of its discontinuous sign function. The scheme replaces this function with the hyperbolic tangent function, $\tanh(\gamma S)$, where γ is a positive constant, thus leading to smoother signals yet retaining convergence characteristics.

6.5 Practical application

An AFSMC with a voltage control strategy can promise much about practical implementation in many robot systems, particularly those that are going to be used in uncertain or varying environments. It becomes a practice in the industry, such as assembly, pick-and-place, and precision handling of materials, in which effects happen from external disturbance and payload changes, since it does not require accurate dynamic modelling, and the computation demands are relatively low. In collaborative robots with human-robot interactions, control is made smooth, replacing the sign function with the hyperbolic tangent function, which creates even safer systems while reducing the stress on mechanical components. The controller becomes an attractive feature to have when it comes to people-robot interactions. High accuracy and adaptability to unmodelled dynamics characterise the method in terms of maximally precise and stable control under biomechanical uncertainties in the application of medical robotics, which comprises surgical assistance and rehabilitation devices. The approach also targets mobile manipulators and service robots, where the efficiency of such processing has not been achieved because it is bounded by storage on board and the unpredictable terrains it tends to encounter during movement.

This voltage-based strategy extends application to affordable, easily measurable signals such as those for the joint position, motor current, and end-effector position, thus promoting application into embedded systems without installing velocity sensors or complicated observers. This kind of practical pedagogy expands its use to teaching platforms and research prototypes, primarily focusing on algorithm development and validation rather than specific and detailed dynamic modelling. Overall, the proposed AFSMC scheme fills the void between robust theoretical research and real-time applicability, a looming candidate for present-day robotic control for academic and industrial interests.

6.6 Limitations and future work

The AFSMC proposed has shown powerful performance and great viability in practice, however, some limitations need to be addressed. The present research is limited to simulation validation on a three-joint robotic arm. The modelled uncertainties and situations for external disturbance in the environment may be apparent but have not yet evaluated the performance of the system in real-world conditions, such as sensor noise, time delay, and actuator saturation. Therefore, the immediate generalisability of the results to practical systems is hampered because there is no physical implementation on a hardware platform. The premise of full state feedback, with end-effector position, joint position, and motor current measurements, is also a limitation. In practice, most applications of low-cost or compact robotics will need additional sensing and estimation schemes to get workspace positions or high-fidelity current readings, adding further

complexity to the system. The fuzzy component, however, is currently implemented with fixed rule structures, although effective in approximating nonlinearities. This could limit its capacity to adapt to conditions in which dynamic time-varying or task-related dynamics vary considerably, especially when the system scales to more complex manipulators with a greater number of degrees of freedom.

Some future work would include developing and validating in real-time an embedded implementation of the proposed controller on a physical robotic platform, including the complete experimentation within realistic operational constraints like joint flexibility, backlash, or communication delays. The sensor fusion and state estimation techniques, for example, observer or extended Kalman filters, may enable the implementation to be carried out in systems with limited sensing. Future work may also study integrating self-organising or neuro-fuzzy systems that adaptively change their fuzzy rule bases during operations into the system for better performance and accuracy. Another exciting future opportunity is to extend the controller to collaborative multi-arm systems with several arms, where inter-arm coordination and mobility constraints could pose an additional layer of complexity. Finally, the proposed voltage-based strategy could be set up against newer intelligent control schemes, such as reinforcement learning or deep adaptive controllers, to measure performance benchmarks for the technology in more uncertain environments.

7 Conclusions

The current study devised an original decentralised AFSMC for a robotic arm by voltage control. Unlike other torque-based methods, the new approach does not depend on an accurate dynamic model for its operation; therefore, it is less computationally demanding than others, yet it provides high tracking accuracy and robustness to external disturbances and uncertainties in the system. Perturbation estimation via FLC for approximation of nonlinear dynamics is combined with a smoothly switching sliding mode control law to robustly mitigate the effects of structured and unstructured uncertainties for a complete and fine end-effector motion control design. Simulations were conducted to validate the theoretical developments and show that the control framework developed strongly outperforms conventional control strategies, with good tracking error reduction, while keeping control efforts to a reasonable limit. Moreover, being voltage-based, the method being discussed finds its place in the realm of real-time embedded low-cost robotics, given its freedom from velocity feedback. In conclusion, the presented AFSMC with voltage control provides an easy, scalable, and theoretically sound approach for robust robotic control in difficult environments. It stands out as a simple, flexible, and reliable candidate for direct deployment in industrial, collaborative, and mobile robotic systems. Future works will include some experimental validations of the proposed control scheme and an effort to enhance the adaptability of the control architecture through intelligent learning-based extensions, thereby enhancing its role in next-generation robotic control architectures.

Acknowledgements

This work was supported by The Research on Industrial Robot Stereoscopic Vision Technology project of science and technology research program of Chongqing Education Commission of China (No KJZD-K202203202).

Declarations

All authors declare that they have no conflicts of interest.

References

Abdel-Sattar, A., El-Sayed, A.H.M., Tawfiek, S.R. and Kassem, A. (2025) 'Optimal sliding surface PID for position control of robotic arm', *Journal of Advanced Engineering Trends*, Vol. 44, No. 1, pp.272–281.

Ariyansyah, Q. and Ma'arif, A. (2023) DC motor speed control with proportional integral derivative (PID) control on the prototype of a mini-submarine', *Journal of Fuzzy Systems and Control*, Vol. 1, No. 1, pp.18–24.

Behnamfar, M., Tariq, M. and Sarwat, A.I. (2024) 'Novel autonomous self-aligning wireless power transfer for improving misalignment', *IEEE Access*, 7 March.

Fateh, M.M. and Khorashadizadeh, S. (2012) 'Robust control of electrically driven robots by adaptive fuzzy estimation of uncertainty', *Nonlinear Dynamics*, August, Vol. 69, pp.1465–1477.

Fateh, M.M. and Soltanpour, M.R. (2009) 'Robust task-space control of robot manipulators under imperfect transformation of control space', *International Journal of Innovative Computing, Information and Control*, Vol. 5, No. 11, pp.3949–3960.

Fazilat, M. and Zioui, N. (2025) 'Quantum-inspired sliding-mode control to enhance the precision and energy efficiency of an articulated industrial robotic arm', *Robotics*, Vol. 14, No. 2, p.14.

Ho, H.F., Wong, Y-K. and Rad, A.B. (2007) 'Robust fuzzy tracking control for robotic manipulators', *Simulation Modelling Practice and Theory*, Vol. 15, No. 7, pp.801–816.

Hu, Q., Wang, Z. and Gao, H. (2008) 'Sliding mode and shaped input vibration control of flexible systems', *IEEE Transactions on Aerospace and Electronic Systems*, Vol. 44, No. 2, pp.503–519.

Jin, T. and Han, X. (2024) 'Robotic arms in precision agriculture: a comprehensive review of the technologies, applications, challenges, and future prospects', *Computers and Electronics in Agriculture*, Vol. 221, No. 6, p.108938.

Kumar, R. and Kumar, K. (2021) 'Design and control of a two-link robotic manipulator: a review', *AIP Conference Proceedings*, Vol. 2358, No. 1.

Liu, A., Zhao, H., Song, T., Liu, Z., Wang, H. and Sun, D. (2021) 'Adaptive control of manipulator based on neural network', *Neural Computing and Applications*, Vol. 33, No. 5, pp.4077–4085.

Mohammadi, F., Mohammadi-Ivatloo, B., Gharehpetian, G.B., Ali, M.H., Wei, W., Erdinç, O. and Shirkhani, M. (2021) 'Robust control strategies for microgrids: a review', *IEEE Systems Journal*, Vol. 16, No. 2, pp.2401–2412.

Nekoukar, V. and Dehkordi, N.M. (2021) 'Robust path tracking of a quadrotor using adaptive fuzzy terminal sliding mode control', *Control Engineering Practice*, Vol. 110, No. 5, p.104763.

Nguyen, H.T. and Sugeno, M. (2012) *Fuzzy Systems: Modeling and Control*, 6 December, Vol. 2, Springer Science and Business Media.

Odry, Á., Fullér, R., Rudas, I.J. and Odry, P. (2020) 'Fuzzy control of self-balancing robots: a control laboratory project', *Computer Applications in Engineering Education*, Vol. 28, No. 3, pp.512–535.

Ruderman, M. (2023) *Analysis and Compensation of Kinetic Friction in Robotic and Mechatronic Control Systems*, 21 September, CRC Press.

Sharkawy, A.B. and Salman, S.A. (2011) 'An adaptive fuzzy sliding mode control scheme for robotic systems', *Intelligent Control and Automation*, Vol. 2, No. 4, pp.299–309.

Ur Rahman Efti, M.A. and Hosen, M.I. (2023) '3DOF intelligent rehabilitation robot design for knee and ankle', *Journal of Artificial Intelligence and System Modelling*, Vol. 1, No. 1, pp.15–31.

Yang, Y., Zhang, H.H. and Voyles, R.M. (2023) 'Optimal fractional-order proportional–integral–derivative control enabling full actuation of decomposed rotary inverted pendulum system', *Transactions of the Institute of Measurement and Control*, Vol. 45, No. 10, pp.1986–1998.

Yin, X., Pan, L. and Cai, S. (2021) 'Robust adaptive fuzzy sliding mode trajectory tracking control for serial robotic manipulators', *Robotics and Computer-Integrated Manufacturing*, 1 December, Vol. 72, p.101884.

Zhu, Q., Mobayen, S., Nemati, H., Zhang, J. and Wei, W. (2023) 'A new configuration of composite nonlinear feedback control for nonlinear systems with input saturation', *Journal of Vibration and Control*, Vol. 29, Nos. 5–6, pp.1417–1430.

Nomenclature

Abbreviation	*Definition*
AFSMC	Adaptive fuzzy sliding mode control
PID	Proportional-integral-derivative
PD	Proportional-derivative
SMC	Sliding mode control
DC	Direct current
DOF	Degree of freedom
IFTSMC	Integral fast terminal sliding mode control
Q-SMC	Quantum sliding mode control
RBF	Radial basis function
ANN	Artificial neural network
FLC	Fuzzy logic controller
SISO	Single input single output
DSP	Digital signal processor
FPGA	Field programmable gate array
EKF	Extended Kalman filter

Symbol	*Description*
K_b	Back-EMF constant matrix
K_m	Motor torque constant matrix
i	Motor current vector
$f(z)$	Nonlinear dynamic term in state-space
S	Sliding surface vector
P	Estimated uncertainty bound vector
μ	Positive gain vector for SMC

Symbol	*Description*
θ	Joint position vector of the robot
$\dot{\theta}$	Joint velocity vector
$\ddot{\theta}$	Joint acceleration vector
$D(\theta)$	Inertia matrix of the robotic arm
$C(\theta,\dot{\theta})$	Coriolis and centrifugal torque vector
$G(\theta)$	Gravitational torque vector
τ	Input torque vector
τ_m	Motor-generated torque vector
θ_m	Motor position vector
J	Motor inertia matrix
B	Motor damping coefficient matrix
r	Gear reduction ratio
$F_s(\theta)$	Dry friction vector
X	End-effector (workspace) position vector
$\dot{X}$	End-effector velocity vector
$J(\theta)$	Jacobian matrix
u	Input voltage vector to the motors
R	Armature resistance matrix
L	Armature inductance matrix
α	Positive-definite gain matrix
$\in$	Fuzzy approximation error
e	Tracking error in workspace